Journal of Biomolecular NMR (2005) 31: 1–9

Simultaneous ^{1}H- or ^{2}H-, ^{15}N- and multiple-band-selective ^{13}C-decoupling during acquisition in ^{13}C-detected experiments with proteins and oligonucleotides

Beat Vögeli[a], Helena Kovacs[b] & Konstantin Pervushin[a,*]
[a]*Laboratorium für Physikalische Chemie, Swiss Federal Institute of Technology, ETH-Hönggerberg, CH-8093 Zürich, Switzerland;* [b]*Bruker BioSpin, Industriestrasse 26, CH-8117 Fällanden, Switzerland*

Received 6 July 2004; Accepted 14 October 2004

Key words: ^{13}C-detected NMR spectroscopy, homonuclear decoupling, multiple-band selective decoupling

Abstract

Significant resolution improvement in ^{13}C,^{13}C-TOCSY spectra of uniformly deuterated and ^{13}C, ^{15}N-labeled protein and ^{13}C,^{15}N-labeled RNA samples is achieved by introduction of multiple-band-selective ^{13}C-homodecoupling applied simultaneously with ^{1}H- or ^{2}H- and ^{15}N-decoupling at all stages of multidimensional experiments including signal acquisition period. The application of single, double or triple band-selective ^{13}C-decoupling in 2D-[^{13}C,^{13}C]-TOCSY experiments during acquisition strongly simplifies the homonuclear splitting pattern. The technical aspects of complex multiple-band homonuclear decoupling and hardware requirements are discussed. The use of this technique (i) facilitates the resonance assignment process as it reduces signal overlap in homonuclear ^{13}C-spectra and (ii) possibly improves the signal-to-noise ratio through multiplet collapse. It can be applied in any ^{13}C-detected experiment.

Introduction

Novel strategies based on ^{13}C-detection of the backbone and side-chain resonances hold promise for expanding NMR structural analysis to large uniformly deuterated proteins (Eletsky et al., 2003; Pervushin and Eletsky, 2003). We have combined ^{13}C- and ^{1}H-detected experiments to obtain the backbone resonance assignment of a 44 kDa protein (Hu et al., 2003; Pervushin and Eletsky, 2003) and designed an approach based on ^{13}C-start, ^{13}C-observe experiments to get a nearly complete assignment of the side-chain ^{13}C resonances of this protein (Eletsky et al., 2003). We have also demonstrated that the ^{13}C-start, ^{13}C-observe experiments can be used to determine multiple side-chain residual ^{13}C–^{13}C dipolar couplings upon partial alignment of a protein (Vögeli et al., 2004). For these studies, a cryogenic probe optimized for ^{13}C-detection was used at 500 MHz. The applicability of these methods is, however, limited by spectral overlap due to the complex splitting patterns of the cross-peaks, which leads to difficulties in assigning the peaks and in extracting single $J_{CC} + D_{CC}$ couplings from them, and to poor signal-to-noise for resonances at large offsets. Similarly, the application of ^{13}C-detected methods to oligonucleotides is compromised by homonuclear couplings particularly in the crowded ribose region. Homodecoupled ^{13}C-detected methods are potentially a useful complement for the resonance assignment of labeled RNA and DNA, particularly in the sugar region where the ^{1}H chemical shift dispersion is low. Bertini and coworkers recently demonstrated band-selective homodecoupling of ^{13}CO from $^{13}C^{\alpha}$ and *vice versa* in the COCAMQ

*To whom correspondence should be addressed. E-mail: kope@phys.chem.ethz.ch

and CT-COSY experiments at 500 MHz (Bermel et al., 2003). Earlier Matsuo et al. have implemented band-selective ^{13}C-decoupling of ^{13}CO and $^{13}C^{\beta}$ during ^{13}C-evolution in the Cbd-HCCH-TOCSY experiment for proteins (Matsuo et al., 1996). Brutscher et al. have applied band-selective ^{13}C-decoupling on C2′, C5′ and low-field aromatic-^{13}C during the ^{13}C-evolution in 2D-[^{1}H,^{13}C]-TROSY and 3D-[^{13}C,^{13}C]-NOESY-[^{1}H,^{13}C]-TROSY experiments on an RNA sample (Brutscher et al., 2001). In this paper, we show that the above mentioned obstacles can be alleviated by employing band-selective ^{13}C-homodecoupling, simultaneously with ^{1}H- or ^{2}H- and ^{15}N-decoupling during all stages of multidimensional experiments including the signal acquisition period. Thus, the approach of ^{13}C-detection becomes attractive for biomolecular NMR-applications, particularly, if it can be combined with the gains in sensitivity and resolution substantiated by cryogenic probes and high magnetic fields as is shown by the present work.

Results

Performance of the band-selective adiabatic inversion pulses was initially tested in 1D ^{1}H- or ^{2}H-decoupled experiments. The experimental inversion profiles are shown in Figures 1 and 2 for the protein and RNA spectra, respectively. In each case, a 1D spectrum lacking a ^{13}C inversion pulse is shown on the top. The calculated excitation profiles for the double- and triple-band pulses are also presented in Figure 1c and d, respectively. The single-band carbonyl ^{13}C-, double-band $^{13}C^{\alpha}/^{13}C^{\gamma}$- and triple-band ^{13}CO/$^{13}C^{\beta}$-inversion pulses for the protein, displayed in Figure 1b–d, and the single-band C2′/C3′- and C4′-selective pulses for the RNA-riboses, displayed in Figure 2b and c, all feature high resonance selectivity. These band-selective inversion pulses were subsequently employed in the homodecoupling trains during acquisition (Hammarström and Otting, 1994) in the 2D-[^{13}C,^{13}C]-TOCSY experiment (Eletsky et al., 2003), depicted in Figure 3. This is, in fact, the most sensitive [^{13}C,^{13}C]-correlation experiment for molecules of current size (Fischer et al., 1996). The p5m4 supercycle (Tycko et al., 1985; Fujiwara and Nagayama, 1988) with a homodecoupling duty cycle of 20% was used in all cases, and the RF field strength of the adiabatic pulses was increased accordingly.

Figure 4 shows relevant expansions of 2D-[^{13}C,^{13}C]-TOCSY spectra of human ubiquitin (Vijaykumar et al., 1987). The different options of band-selective homonuclear ^{13}C-decoupling, all of which were applied together with ^{2}H- and ^{15}N-decoupling at 900 MHz, are compared to a reference spectrum recorded with ^{2}H-decoupling only. The single-band selective ^{13}CO-decoupling collapses the carbonyl-coupling for all $^{13}C^{\alpha}$ cross-peaks (Figure 4a) and the sidechain-carbonyl coupling in asparagines and glutamines. Figures 5c–e show representative slices for C^{α}/C^{β} of ASN60, C^{β}/C^{α} of GLN62 and C^{β}/C^{α} of THR22, respectively. The performance of the double-band selective $^{13}C^{\alpha}/^{13}C^{\gamma}$-decoupling is slighty less clean (Figure 4b). Most $^{13}C^{\beta}$ and $^{13}C^{\delta}$ cross-peaks turn into singlets, as illustrated by Figures 5a and b displaying C^{β}/C^{δ} of ARG54 and C^{α}/C^{β} of LEU50, respectively. Figure 5a also depicts the collapse of the coupling from the side-chain ^{15}N in arginine. A minor fraction reveals reduced doublet structure although the coupled spins resonate within the decoupled frequency range, for instance the cross-peak C^{γ}/C^{β} of LEU50. This is even more the case for the triple band selective decoupling of ^{13}CO/$^{13}C^{\beta}$ (Figure 4c). For instance, the cross-peak C^{β}/C^{α} of THR22, which becomes a singlet, in contrast to C^{γ}/C^{α} of GLN62, which remains a reduced doublet, as shown in Figures 5e and d, respectively. Most rewardingly, there are also some cross-peaks such as C^{γ}/C^{β} of LEU50, which become visible only upon $^{13}C^{\alpha}/^{13}C^{\gamma}/^{15}$N-decoupling (Figure 5f).

Figure 6 shows relevant expansions of 2D-[^{13}C,^{13}C]-TOCSY spectra of the RNA 14-mer. The two different band-selective homonuclear ^{13}C-decoupling options are compared to a coupled reference spectrum. All these spectra were recorded with ^{1}H-decoupling at 500 MHz using a ^{13}C-observe CryoProbe. The band-selective ^{13}C-decoupling of C2′ and C3′ collapses the C2′ coupling for all C1′ cross-peaks and C3′ couplings for C4′ cross-peaks, respectively (Figure 6a). The ambiguities due to overlap in the C1′ region between 90 and 92 ppm and in the C4′ region between 78 and 81 ppm in the coupled spectrum could be resolved. The band-selective ^{13}C-decoupling of C4′ collapses the C4′ couplings

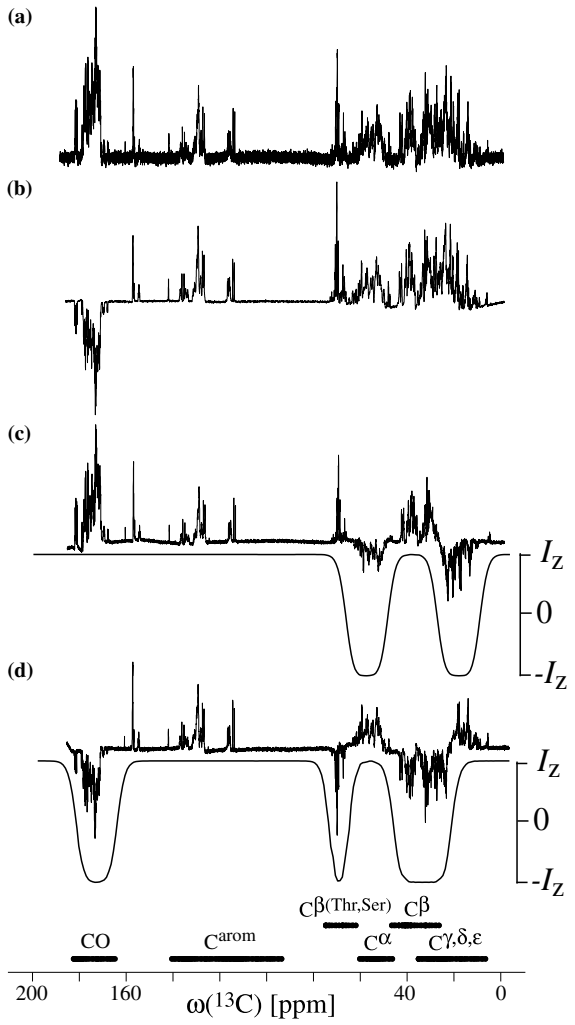

Figure 1. 1D ^{13}C-spectra of a 0.4 mM uniformly ^{2}H,^{15}N,^{13}C-labeled ubiquitin sample measured using a Bruker Avance 900 spectrometer operating at $\gamma B_0(^{1}H) = 900$ MHz. The spectra were recorded using WALTZ16 ^{2}H-decoupling at $\gamma B_1(^{2}H) = 0.83$ kHz during data acquisition. The spectra are superimposed with the inversion profiles of I_z magnetization calculated with the program NMRSIM (Bruker BioSpin). (a) Reference spectrum recorded using a single broad band ^{13}C 90° excitation pulse. (b) 4 ms CO-band-selective inversion CHIRP (Böhlen and Bodenhausen, 1993) pulse with $\gamma B_1(^{13}C) = 1.26$ kHz inverting resonances in the CO region, (c) double-band selective CHIRP pulse of 4 ms length with $\gamma B_1(^{13}C) = 1.75$ kHz inverting the C^{α} and C^{γ} regions and, (d) triple-band selective CHIRP pulse of 4 ms length with $\gamma B_1(^{13}C) = 3.51$ kHz inverting the CO and two C^{β} regions, were applied prior to the 90° excitation pulse. The spectra (a) and (b)–(d) were recorded using 132 and 1024 scans, respectively, with 1s interscan delay.

for all C3′ and C5′ cross-peaks (Figure 6b), resolving particularly the overlap in the C5′ region between 61 and 63 ppm and in the C2′ region between 71 and 73 ppm. Hence these spectra enabled us to confirm the heteronuclear resonance assignment of the complete spin systems of the riboses (Fürtig et al., 2004). On the top of each spectrum, slices taken along the direct dimension (at 75 ppm in the indirect dimension) offer a comparison between the decoupled and the reference spectra.

Discussion

For the homodecoupled 2D [^{13}C,^{13}C]-TOCSY spectra presented in Figure 4, the theoretical S/N improvement of $2 \times 0.894 = 1.789$ per collapsed ^{13}C-doublet is not always achieved experimentally. The factor of 0.894 is the theoretical attenuation due to homonuclear decoupling during acquisition with a 20% duty cycle (Bermel et al., 2003; see also Materials and methods). Although

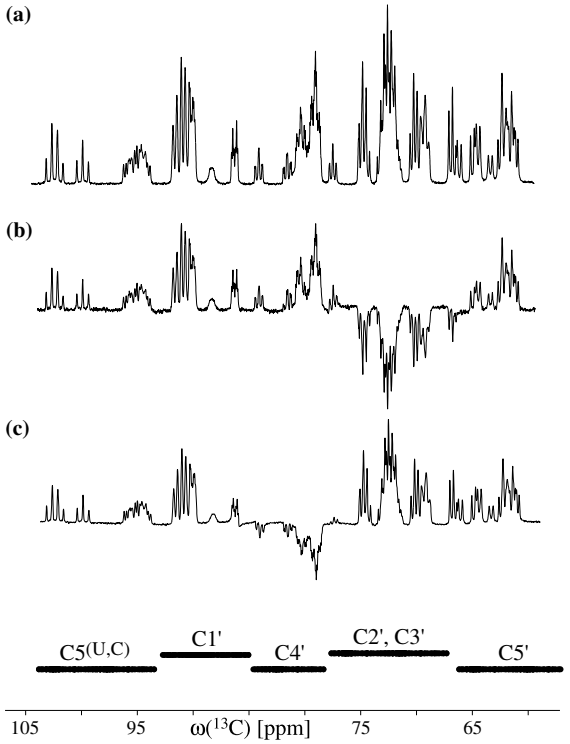

Figure 2. 1D ^{13}C-spectra of ^{15}N,^{13}C-labeled RNA 14-mer, 5′ GGCACUUCGGUGCC 3′, measured using a Bruker Avance 500 spectrometer operating at $\gamma B_0(^1H) = 500$ MHz. The spectra were recorded using WALTZ-16 ^{1}H-decoupling at $\gamma B_1(^1H) = 2.50$ kHz during data acquisition. (a) Reference spectrum recorded using a single broadband ^{13}C 90 ° excitation pulse. (b) 15 ms band-selective inversion CHIRP pulse with $\gamma B_1(^{13}C) = 0.28$ kHz inverting resonances in the C2′ and C3′ region, and, (c) band-selective CHIRP pulse of 20 ms length with $\gamma B_1(^{13}C) = 0.21$ kHz inverting the C4′ region, were applied prior to the 90° excitation pulse. The spectra (a), (b) and (c) were recorded using 512, 322 and 242 scans and 2s, 2s and 1s interscan delay, respectively.

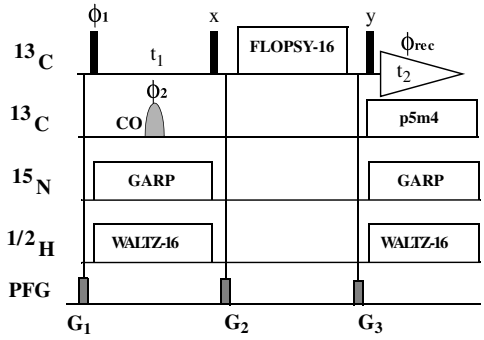

Figure 3. Experimental scheme of the ^{2}H,^{15}N,^{13}C(selective)-decoupled [^{13}C,^{13}C]-TOCSY. Black bars represent broadband ^{13}C 90° pulses. The curved shape indicates a selective, 5%-truncated Gaussian 180° pulse on ^{13}CO with a duration of 100 μsec. The FLOPSY-16 mixing was applied with $\gamma B_1(^{13}C) = 8.3$ kHz with $\tau_{mix} = 16.96$ ms at 900 MHz and with $\gamma B_1(^{13}C) = 10.0$ kHz with $\tau_{mix} = 18.84$ ms at 500 MHz. The boxes on the line labeled PFG indicate sine-shaped pulsed magnetic field gradients along the *z*-axis:G1 and G3, 25 G cm^{-1}, 1 ms; G2, 30 G cm^{-1}, 0.6 ms. The phase cycle is $\phi_1 = \{x, -x, x, -x\}$; $\phi_2 = \{x, x, -x, -x\}$; $\phi_{rec} = \{x, -x, x, -x\}$. ^{2}H- and ^{15}N-decoupling is performed with WALTZ-16 (Shaka et al., 1983) and GARP4 (Shaka et al., 1985) pulse trains, respectively. The homonuclear decoupling employs a p5m4 supercycle (Tycko et al., 1985; Fujiwara and Nagayama, 1988) consisting of single ^{13}CO-, double $^{13}C^{\alpha}/^{13}C^{\gamma}$- or triple ^{13}CO/$^{13}C^{\beta}$-bandselective pulses using CHIRP inversion pulses as described in Figures 1 and 2, with the exception that all rf-power settings were increased by 14 dB to account for the 20% homodecoupling duty cycle.

the comparison to the reference spectrum may not hold exactly due to slightly different experimental settings and the mostly not perfectly resolved single components in the splitting pattern, we estimated the gain factor of the S/N ratio for several peaks. Values ranging roughly from 1.0 to 1.8 per decoupled doublet indicate a rather large distribution in decoupling efficiency and S/N loss.

Initial tests on a ^{13}C,^{15}N-labeled glycine sample indicated clean decoupling of the ^{13}CO- and ^{15}N-spins under simultaneous irradiation of ^{13}C, ^{15}N and ^{2}H (spectra not shown). The collapse of the $^{13}C^{\alpha}$-quadruplet in glycine due to $J_{C\alpha CO}$ and $J_{C\alpha N}$ couplings results, however, in only a twofold gain in signal intensity instead of the expected value of $4 \times 0.894 = 3.578$. An experiment with only ^{15}N- and ^{2}H-decoupling suffers from almost the same loss of intensity, whereas additional ^{13}C-decoupling does not scale the signal intensity by more than the factor of 0.894 ($2 \times 0.894 = 1.789$ per collapsed doublet). Because no spurious noise stemming from decoupling is added, we attribute this loss of signal intensity to heteronuclear interference. In order to minimize heteronuclear interference, we employed the latest type of band-pass frequency filters. Nevertheless, because the relations between the gyromagnetic ratios are $\gamma_C{:}\gamma_N{:}\gamma_D = 1.00{:}0.40{:}0.61$, the sum of ^{15}N and ^{2}H frequencies can interfere with ^{13}C frequencies. Subsequent 1-dimensional test experiments indicated that the S/N loss can be reduced by using less decoupling power on both ^{2}H and ^{15}N. Certainly, this is only applicable in the cases where a weaker decoupling field is acceptable.

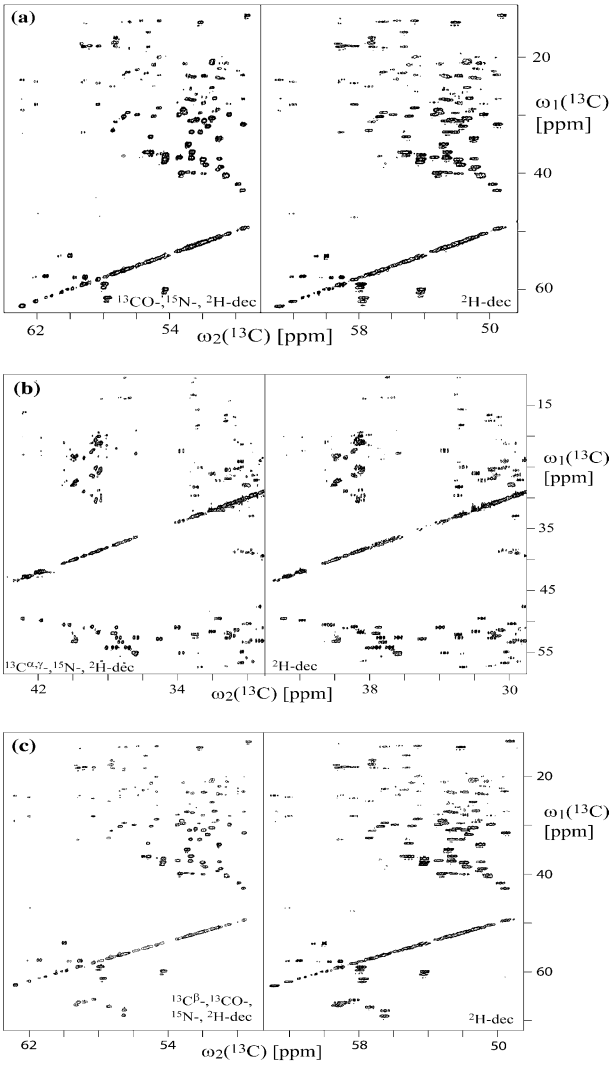

Figure 4. Expansions of 2D-[^{13}C,^{13}C]-TOCSY spectra of uniformly ^{2}H,^{15}N,^{13}C-labeled ubiquitin samples measured at a Bruker Avance spectrometer operating at $\gamma B_0(^1H) = 900$ MHz using ^{2}H,^{15}N,^{13}C-tunable ^{13}C-detection probe (DUX). The right panels show expansions of a reference spectrum with only ^{2}H-decoupling using WALTZ-16 pulse trains at $\gamma B_1 = 0.96$ kHz, $t_{1max} = 11.0$ ms and $t_{2max} = 147.5$ ms and 400×4096 complex points resulting in an acquisition time of 20 h. The left panels show expansions of the multiple-band decoupled spectra: (a) ^{2}H-decoupling using WALTZ-16 pulse trains at $\gamma B_1 = 0.83$ kHz, ^{15}N-decoupling using GARP pulse trains at $\gamma B_1 = 1.3$ kHz, ^{13}C-homonuclear decoupling of CO using a p5m4 supercycle with an adiabatic CHIRP pulse of 4 ms length and 20% smoothing according to Figure 1b, $t_{1max} = 7.1$ ms and $t_{2max} = 147.5$ ms, 256×8192 complex points were collected resulting in an acquisition time of 15 h. (b) ^{2}H-decoupling using WALTZ-16 pulse trains at $\gamma B_1 = 0.96$ kHz, ^{15}N-decoupling using GARP pulse trains at $\gamma B_1 = 1.3$ kHz, ^{13}C-homonuclear decoupling of C^{α} and C^{γ} using a p5m4 supercycle with a double-band selective CHIRP pulse of 4 ms length and 20% smoothing according to Figure 1c, $t_{1max} = 11.0$ ms and $t_{2max} = 147.5$ ms, $400' \times 8192$ complex points were recorded resulting in an acquisition time of 24 h. (c) ^{2}H-decoupling using WALTZ-16 pulse trains at $\gamma B_1 = 0.96$ kHz, ^{15}N-decoupling using GARP pulse trains at $\gamma B_1 = 1.3$ kHz, ^{13}C-homonuclear decoupling of CO and C^{β} using a p5m4 supercycle with a triple-band selective adiabatic CHIRP pulse of 4 ms length and 20% smoothing according to Figure 1d, $t_{1max} = 11.0$ ms and $t_{2max} = 147.5$ ms, 400×8192 complex points were collected resulting in an acquisition time of 35 h. The ^{13}C-homodecoupling was applied with 20% duty cycle in all cases. In all experiments the interscan delay was 1.5 s, the radio-frequency carrier offsets were placed at 40 ppm (^{13}C), 174 ppm (^{13}CO), 120.0 ppm (^{15}N) and 3.0 ppm (^{2}H) and the time domain data were multiplied with a cosine function in the t_1 and t_2 dimensions and zero-filled to 1024 and 16384 points, respectively. 1D slices of six representative cross-peaks are shown in Figure 5.

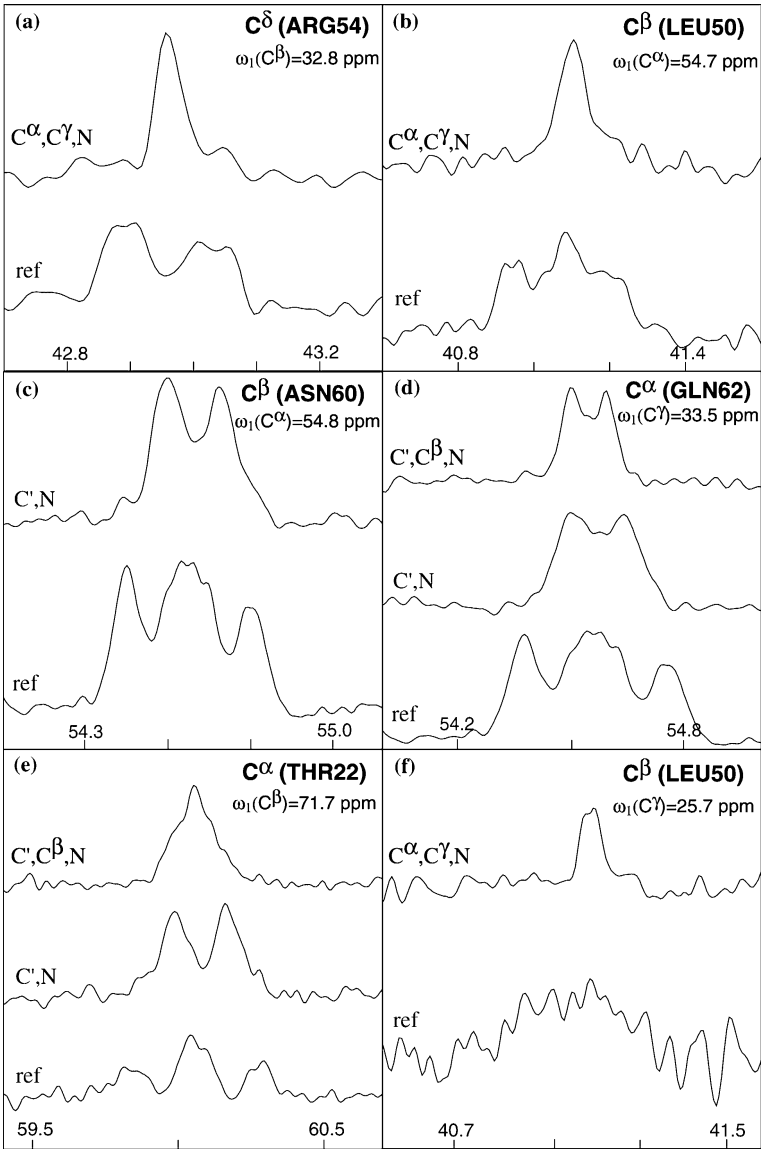

Figure 5. 1D slices of six representative cross-peaks taken along the direct $^{13}C(\omega_2)$ dimension from the spectra shown in Figure 4. Cross-peak assignments are given in the upper right corners. The top slices are taken from [^{13}C,^{13}C]-TOCSY spectra acquired with ^{2}H-, ^{15}N- and band-selective ^{13}C-decoupling as specified on each slice. The bottom slices were recorded with ^{2}H-decoupling only.

For the RNA ribose spectra presented in Figure 6 neither ^{15}N- nor ^{2}H-decoupling was needed. The S/N ratio of the decoupled spectrum is comparable to that of the reference spectrum. The recording times were similar, the interscan delay, however, was 1s in the reference spectrum, whereas 2s was used in the decoupled spectra. The average longitudinal relaxation rate R_1 of C1′ in this molecule is 3.4 Hz at 500 MHz (Radovan Fiala, unpublished results). Based on this value, the S/N is estimated to increase by 36% upon shortening the interscan delay from 2s to 1s (Pervushin et al., 2002). Therefore, for the reference spectrum with an interscan delay of 1s and the decoupled spectra with an interscan delay of 2s, if recorded equally long, the S/N ratios become comparable. This corresponds to the observation in the quantitative 1D tests on the glycine sample, where the S/N ratio was not further

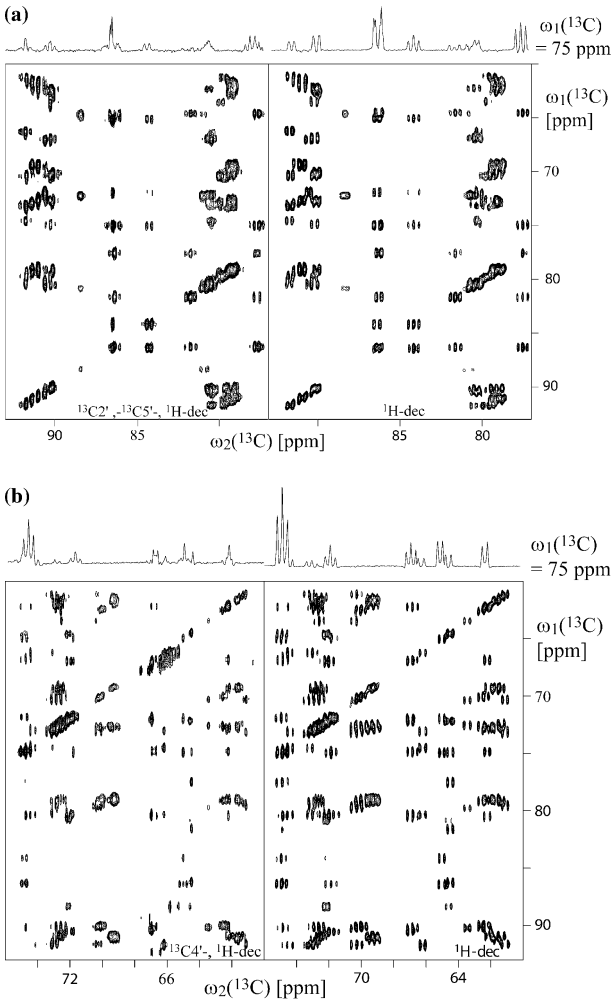

Figure 6. Expansions of 2D-[^{13}C,^{13}C]-TOCSY spectra measured with ^{15}N,^{13}C-labeled RNA 14-mer, 5′ GGCACUUCGGUGCC 3′, recorded on a Bruker Avance spectrometer operating at a proton frequency of 500 MHz and using the 5 mm ^{13}C-observe CryoProbe (DUL). Reference experiments (right): ^{1}H-decoupling using WALTZ-16 pulse trains at $\gamma B_1 = 3.33$ kHz, radio-frequency carrier offsets placed at 110 ppm (^{13}C) and 4.0 ppm (^{1}H), $t_{1max} = 8.0$ ms and $t_{2max} = 116.3$ ms, interscan delay 1.0 s and 284×4096 complex points resulting in an acquisition time of 36 h. Homodecoupled spectra (left): (a) ^{13}C-homonuclear decoupling of C2′ and C3′ using a p5m4 supercycle with an adiabatic CHIRP pulse of 15 ms length and 20% smoothing according to Figure 1b, the radio-frequency carrier offsets were placed at 82 pm (^{13}C), 71 pm (^{13}C-decoupling channel) and 4.0 pm (^{1}H). (b) ^{13}C-homonuclear decoupling of C4′ using a p5m4 supercycle with an adiabatic CHIRP pulse of 20 s length and 20% smoothing according to Fig. 1c, the radio-frequency carrier offsets were placed at 79 pm (^{13}C), 81.5 pm (^{13}C-decoupling channel) and 4.0 pm (^{1}H). In both homodecoupled spectra ^{1}H-decoupling was applied using WALTZ-16 pulse trains at $\gamma B_1 = 2.50$ kHz. Both spectra were recorded with $t_{1max} = 8.0$ ms, $t_{2max} = 163.8$ ms, 100×2048 complex points and an interscan delay of 2.0 s. The acquisition time was 31 h (a) and 36 h (b), respectively. The time domain data of all spectra was multiplied with a cosine function in the t_1 and t_2 dimensions and zero-filled to 1024 and 4096 points, respectively.

downscaled than by the theoretical factor upon switching on homonuclear ^{13}C-decoupling (but no simultaneous ^{2}H- and ^{15}N-decoupling, see above).

In fact, the ^{13}C-homodecoupling could also be used to simplify extraction of scalar and residual dipolar couplings, J_{CC} and D_{CC}, in complex spin systems. However, if the frequency of one of the spins involved in the nondecoupled splitting lies in the transition region of the excited range, rescaling of the apparent splitting is expected (Freeman, 1986). More investigation is required to evaluate the reliability of extracted J_{CC} and D_{CC} values.

Conclusions

The current homodecoupling technique proves to be a useful complement to ^{13}C-detection based experiments. The use of the technique (i) facilitates the resonance assignment process. Signal overlap is reduced due to line narrowing and collapsing of multiplet pattern in homonuclear spectra. (ii) Because application of ^{13}C-decoupling solely (or together with ^{2}H) yields S/N comparable to S/N in the reference spectra, collapsed multiplets result in higher signal intensity. However, simultaneous decoupling of ^{2}H and ^{15}N sacrifices some of the S/N. The homodecoupling technique can be applied in any ^{13}C-detected experiment. In order to further reduce the spectral overlap in ^{13}C-detected experiments, we currently develop experiments which utilize several magnetization transfer steps and make use of spin-state editing. Thus, direct ^{13}C-detection in perdeuterated proteins for resonance assignment and extraction of a large number of side-chain ^{13}C–^{13}C RDC constraints is becoming a useful complement to high quality structure determination. We also pursue ^{13}C-detection as an alternative means to obtain signal assignment and structural constraints for oligonucleotides.

Materials and methods

The experiments at 500 MHz were performed with a Bruker Avance spectrometer equipped with a cryogenic Z-gradient DUL ^{13}C{^{1}H, ^{2}H} probe, which is optimized for ^{13}C-detection. With this probe, however, ^{15}N-decoupling is not possible. The sample was 2 mM ^{15}N,^{13}C-labeled RNA 14-mer, 5′ GGCACUUCGGUGCC 3′ (produced by Silantes; Fürtig et al., 2004), dissolved in 90%/10% H_2O/D_2O at 295 K. The experiments at 900 MHz were performed with a Bruker Avance spectrometer equipped with a conventional Z-gradient DUX ^{13}C{^{15}N, ^{2}H} probe, which is optimized for ^{13}C-detection. With this probe, ^{1}H-decoupling is not possible. The sample was 1.6 mM ^{2}H,^{13}C,^{15}N-labeled (98% isotope enrichment) non-tagged human ubiquitin sample dissolved in 88%/12% H_2O/D_2O at pH 7.3 and 295 K.

The multiple band-selective adiabatic pulses were created through (i) integration of the corresponding frequency bands in a 1D spectrum to define the adiabatic sweep width and (ii) determination of the pulse length and power by using the ShapeTool in the software package XWIN-NMR 3.5 (Bruker BioSpin). In all cases, the adiabatic pulse shape CHIRP (Böhlen and Bodenhausen, 1993) was used, with 20% smoothing and a sweep from low to high field. If created through integration the resulting pulse directly becomes a sum of the band-selective inversion pulses with phase modulations according to the appropriate offset frequencies.

Figure 7 shows schematically the implementation of the complex multiband homodecoupling during signal acquisition. The homodecoupling duty cycle (HDDUTY) is calculated as $p/(r + p) \times 100\%$, where p is the irradiation time and $r = (\text{dwell time}) - p$. While switching on the decoupling pulse, 1/3 of the delay between points (v_1) is lost after the last measured point pair. After the last unmeasured point pairs, the pulse is still applied for 1/6 of the delay between points (v_2). v_1 and v_2 are indicated by grey boxes. Thus, the number of lost points (open dots) amounts to all the points in the time window $p + v_1 + v_2$ and the points in the time window $r - v_1 - v_2$ contribute effectively to the signal (black dots). The signal-to-noise S/N as a function of the signal-to-noise in an experiment without decoupling $(S/N)_C$ is

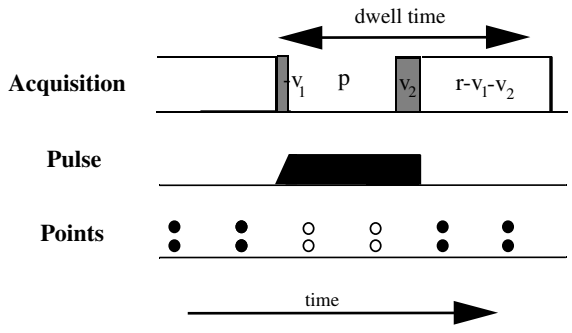

Figure 7. Dwell cycle showing the acquisition status, the pulse p and the dwell window on the time axis. Filled and empty circles represent data acquisition points respectively contributing and not contributing to the signal. Time periods v_i, $I = 1,2$ are discussed in the text.

$$S/N = \sqrt{\frac{W(r - v_1 - v_2)}{W\ (\text{dwell time})}} \cdot (S/N)_c$$
$$\approx \sqrt{\frac{100\% - \text{HDDUTY}}{100\%}} \cdot (S/N)_c,$$

where $W(t)$ is the number of points within the time window of length t.

The dwell time was 18 μs in the protein experiments and 80 μs in the RNA experiments, and the total number of points within a dwell time was 6 and 32, respectively. 20% HDDUTY yields a downscale factor of 0.894, which is a gain of 1.789 for a decoupled doublet. Twenty percent is a reasonable compromise between the loss in S/N and decoupling power. According to the convolution theorem in Fourier transformation, an irradiation period of total length p spaced by r and with $p \ll r$ in the time domain, produces signals with sidebands spaced by n/r (n = integer) in the frequency domain (Morris and Freeman, 1978). Because the dwell time is less than 100 μs in all experiments, the first sidebands on both sides of the excitation region appear more than 10 kHz away from the irradiation frequency.

Acknowledgements

Financial support was obtained from the Swiss National Science Foundation grant to K.P. We gratefully acknowledge helpful discussions with Dr Fred Damberger, Dr Wolfgang Bermel, Dr Detlef Moskau, Dr Gerhard Eber and Dr Donghan Lee.

References

Bermel, W., Bertini, I., Felli, I.C., Kümmerle, R. and Pierattelli, R. (2003) *J. Am. Chem. Soc.*, **125**, 16423–16429.

Böhlen, J.M. and Bodenhausen, G. (1993) *J. Magn. Reson. Ser. A*, **102**, 293–301.

Brutscher, B., Boisbouvier, J., Kupce, E., Tisne, C., Dardel, F., Marion, D. and Simorre, J.P. (2001) *J. Biomol. NMR*, **19**, 141–151.

Eletsky, A., Moreira, O., Kovacs, H. and Pervushin, K. (2003) *J. Biomol. NMR*, **26**, 167–179.

Fischer, M.W.F., Zeng, L. and Zuiderweg, E.R.P. (1996) *J. Am. Chem. Soc.*, **118**, 12457–12458.

Freeman, R. (1986) *Handbook of Nuclear Magnetic Resonance,* Longman Scientific & Technical, Essex.

Fujiwara, T. and Nagayama, K. (1988) *J. Magn. Reson.*, **77**, 53–63.

Fürtig, B., Richter, C., Bermel, W. and Schwalbe, H. (2004) *J. Biomol. NMR*, **28**, 69–79.

Hammarström, A. and Otting, G. (1994) *J. Am. Chem. Soc.*, **116**, 8847–8848.

Hu, K., Eletsky, A. and Pervushin, K. (2003) *J. Biomol. NMR*, **26**, 69–77.

Matsuo, H., Kupce, E. and Wagner, G. (1996) *J. Magn. Reson. B*, **113,** 190–194.

Morris, G.A. and Freeman, R. (1978) *J. Magn. Reson.*, **29**, 433–462.

Pervushin, K. and Eletsky, A. (2003) *J. Biomol. NMR*, **25**, 147–152.

Pervushin, K., Vögeli, B. and Eletsky, A. (2002) *J. Am. Chem. Soc.*, **124**, 12898–12902.

Shaka, A.J., Barker, P.B. and Freeman, R. (1985) *J. Magn. Reson.*, **64**, 547–552.

Shaka, A.J., Keeler, J., Frenkiel, T. and Freeman, R. (1983) *J. Magn. Reson.*, **52**, 335–338.

Tycko, R., Pines, A. and Guckenheimer, J. (1985) *J. Chem. Phys.*, **83**, 2775–2802.

Vijaykumar, S., Bugg, C.E. and Cook, W.J. (1987) *J. Mol. Biol.*, **194**, 531–544.

Vögeli, B., Kovacs, H. and Pervushin, K. (2004) *J. Am. Chem. Soc.*, **126**, 2414–2420.